Magnetic field influenced electron-impurity scattering and magnetotransport

Jingjing Feng, Cong Xiao, Yang Gao, and Qian Niu

Phys. Rev. B **100**, 134202 — Published 9 October 2019

DOI: 10.1103/PhysRevB.100.134202

Magnetic field influenced electron-impurity scattering and magnetotransport

Jingjing Feng, Cong Xiao, Yang Gao, and Qian Niu
Department of Physics, The University of Texas at Austin, Austin, Texas 78712, USA
(Dated: September 24, 2019)

We formulate a classical theory ($\omega_c\tau \lesssim 1$ with ω_c as the cyclotron frequency and τ as the relaxation time) to study the influence of perpendicular magnetic field on the electron-impurity scattering process in the two-dimensional electron gas. To describe the curved incoming and outgoing trajectories, we introduce a general recipe based on an abstraction of the actual impurity scattering process to define the scattering parameters such as the incoming and outgoing momentum and coordinate jump. In this picture, we can conveniently describe the skew scattering and coordinate jump, which will eventually modify the Boltzmann equation. We find an anomalous Hall resistivity different from the conventional Boltzmann-Drude result and a negative magnetoresistivity as a parabolic function of magnetic field. The origin of these results is analyzed. The relevance between our theory and recent simulation and experimental works are also discussed.

I. INTRODUCTION

Magneto-transport of two-dimensional electrons is an interesting but yet complicated topic in condensed matter physics. Its various behaviors, such as the Shubnikov-de Haas oscillation [1], quantum Hall conductance [1], linear magnetoresistance [2], etc., contain a wealth of information about the underlying systems. However, one of the simplest questions in this field, i.e., how the electron transports through disordered materials under a magnetic field in the classical regime, has not been fully understood yet.

In the classical ($\omega_c\tau \lesssim 1$) regime, the electron transport can be generally described by the Boltzmann equation [3]. However, it has been pointed out that the Boltzmann equation has to be revised to incorporate the memory effect (also called non-Markovian effect [4–9]) resulting from the bending of electronic trajectories by the Lorentz force. There are two configurations of memory effect, i.e. either repeatedly scattering on the same impurity, or repeatedly passing through a region without scattering (the latter one is also called Corridor effect [4–7]). In addition to the memory effect, there is an equally important issue that needs to be addressed, i.e. how the magnetic field affects a single electron-impurity scattering event. This problem shares the same origin with the memory effect - bending trajectories, but solves for one-time scattering configuration, in contrast to the two configurations of memory effect. This problem has a fundamental difficulty in defining scattering parameters as the incoming and outgoing asymptotic trajectories are bent by the magnetic field.

In this work, we introduce a general recipe based on an abstraction of the actual impurity scattering process to define scattering parameters for the single elastic impurity scattering. It yields the conventional scattering parameters in the absence of the magnetic field. More importantly, it can introduce an appropriate set of scattering parameters in the presence of magnetic field to calculate the differential cross section. Specifically, the real scattering process can be abstracted into a sudden switch between the initial asymptotic and final asymptotic trajectory. In this classical picture, we can conveniently describe the skew scattering [10] and coordinate jump [11], which will eventually modify the Boltzmann equation. We then apply this recipe to the two-dimensional Lorentz model [12] where free electrons are subject to in-plane electric field and out-of-plane magnetic field, and scattered by randomly distributed hard-disk impurities.

We show the following results. 1) The magnetoresistivity is a negative parabolic function of magnetic field. Our result, together with the one from the previous theory of corridor effect [7] yields a more accurate magnetoresistivity, closer to the numerical result [6]. 2) The obtained Hall coefficient becomes magnetic field-dependent, deviating from the Drude theory. For experiments, this deviation needs to be taken into account when converting the measured Hall coefficients to real electron densities. 3) The longitudinal relaxation time obtained in our theory depends on magnetic field which deviates from the Drude theory.

This paper is organized in the following way. In Section II, we present the general recipe to define scattering parameters for the impurity scattering, and use it to discuss the skew scattering and coordinate jump under magnetic field. The conventional Boltzmann equation is thus modified by these two mechanisms in the linear response regime [13]. In Section III, we solve the modified Boltzmann equation for the two-dimensional Lorentz model and derive the anomalous Hall resistivity and negative magnetoresistivity. In Section IV we compare our result with relevant simulations and experiments. Finally, we introduce a phenomenological method to include skew scattering into the Drude model.

II. CLASSICAL THEORY OF IMPURITY SCATTERING AND ELECTRON TRANSPORT UNDER MAGNETIC FIELD

In this section, we will formulate a classical theory of impurity scattering and electron transport in two-dimensional plane influenced by the external perpendicular magnetic field. Our theory only considers a single

scattering event and neglects the well-studied memory effect, correlation effect and localization effect [22]. One possible application of our theory is the electron transport in randomly distributed two-dimensional anti-dots under magnetic field. The anti-dots are geometrical holes punched into two dimensional electron gas (2DEG) on semiconductor GaAs [14–16, 21].

Our theory requires that the impurity characteristic size a is much smaller than the mean free path l, which is further smaller than the cyclotron radius R. This condition is due to the following assumptions. First, we assume a central scattering potential with a characteristic length scale a for a single scatterer. Second, our theory is developed under dilute limit of impurity concentration $n_i a^2 \ll 1$ (where n_i is impurity density), and we only consider the single impurity scattering. This condition also suggests that $a \ll l$ with l being the mean free path, due to the fact that $n_i a^2 = a/l$. Third, from the classical regime $\omega_c \tau \lesssim 1$ (where ω_c is cyclotron frequency, and τ is relaxation time), the cyclotron radius R is larger than the mean free path, i.e. $R > l$. Summing up all the above requirement, the pre-condition of our theory is $a \ll l < R$. We note that this condition is the same with that for the corridor effect in literatures [6, 7].

The derivation and discussion in this section are organized as follows. First, we review a critical issue in formulating our theory: as the incoming and outgoing asymptotic trajectories are bent by the magnetic field, it is not clear how to parameterize them. To resolve this issue, we introduce a general recipe to redefine the impact parameter, the incoming and outgoing momentum, and the scattering angle. Then we use them to naturally describe and calculate the skew-scattering and coordinate jump at the presence of the magnetic field, which will eventually modify the Boltzmann transport equation.

A. Abstraction of impurity scattering process

Our final goal is to study the electron transport under magnetic field in a classical picture. Therefore, we will use the Boltzmann transport equation. It contains two parts: one describes the electron drifting between collisions driven by external forces, and the other one describes the electron scattering off impurities that leads to electronic steady states. In our situation, the drifting part is simply driven by the Lorentz force, which is well known. Therefore, we will focus on the impurity scattering under magnetic field.

There is a critical issue in describing such a scattering process classically. To see this, we first review the conventional electron-impurity scattering in the absence of the magnetic field. In Fig. 1, we plot such a scattering process. The real electron trajectory is represented by the solid curve, with the arrow showing the direction of the electron motion. Then scattering parameters such as the impact parameter, the incoming and outgoing momentum, and the scattering angle are easily defined from the incoming and outgoing asymptotic trajectories, as illustrated in Fig. 1. In the presence of a constant out-of-plane magnetic field, however, such definition of scattering parameters does not work, because the above quantities vary in time in the asymptotic sense due to the curved incoming and outgoing asymptotic trajectories.

To resolve this issue, we propose a recipe to define those scattering parameters generally. First, we introduce the abstraction of the impurity scattering process. It proceeds as follows: we assume the scattering occurs suddenly at the time $t = 0$; we then use the asymptotic trajectories as $t \to -\infty$ and $t \to \infty$ to replace the true trajectory at $t < 0$ and at $t > 0$, respectively. We call those imaginary trajectories as the initial and final asymptote, respectively. We define this method as the abstraction of the impurity scattering process, as it only keeps the essence of the scattering process, i.e. the transition from the initial asymptote to the final asymptote, and abstract the detail of the transition as a sudden switch.

There is a degree of freedom in the above procedure. Note that even though we have restricted the scattering to occur at $t = 0$, this point itself is not well defined. In other words, we have the freedom to define this artificial point. For a central scattering potential, we can fix this issue by requiring that at $t = 0$ the electron reaches the point in the initial asymptote closest to the scatter. We call this point the starting point (represented by the red dot in Fig. 1). If the scattering potential respects the rotational symmetry, the starting point in different initial asymptotes form a straight line called the event

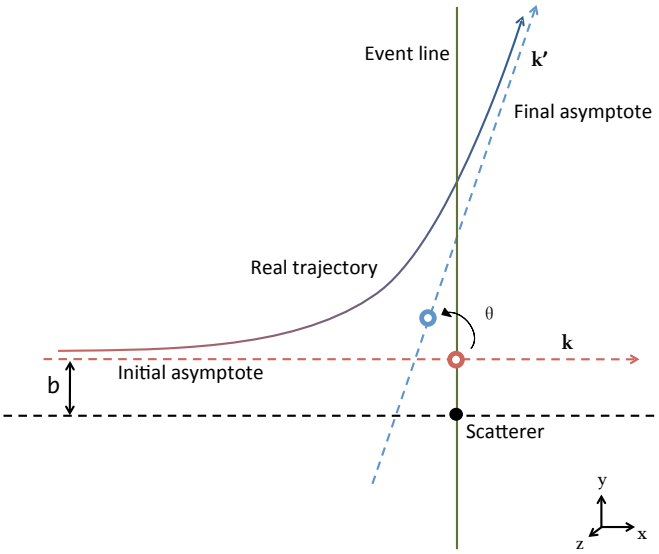

FIG. 1. The illustration of a general scattering process without magnetic field. The solid curve is the real trajectory starting from color red and ending with color blue. The red and blue dashed lines are the initial and final asymptotic trajectory, respectively. The red and blue empty dot are the starting point and ending point, respectively. The green line is the event line passing through starting point and impurity center.

line which marks the occurring of scattering event as illustrated in Fig. 1. It turns out that the event line is orthogonal to the initial asymptotes and passes the center of the scatterer.

With the help of the abstraction of the impurity scattering process, we define the scattering parameters as follows. We define the distance between the starting point and the scattering center to be the impact parameter, the momentum at $t = 0_-$ and $t = 0_+$ to be the incoming and outgoing momentum, respectively, and the angle between the incoming and outgoing momentum to be the scattering angle. Those scattering parameters reduce to the conventional ones in the absence of the magnetic field, as shown in Fig. 1. We further define the point in the final asymptote at $t = 0_+$ to be the ending point (represented by the blue dot in Fig. 1). This definition of scattering parameters is clearly independent of the scattering details and works for any type of the initial and final asymptotes.

Using the above concepts, the abstraction of the scattering process can be concisely stated as follows: the electron moves along the initial asymptote to the starting point, gets scattered to the ending point and finally moves away from the scatterer along the final asymptote.

B. Application to hard disk potential

We first apply the abstraction of the scattering process to hard disk potential in the absence of magnetic field. By applying to this fully known case, we aims at a necessity check of the correctness of our theory. Consider an electron incident on a hard disk potential with straight line trajectory (Fig. 2). The real trajectory (solid lines) changes its direction after the electron hits the scatterer. However, the initial and final asymptote (dashed lines) can be elongated along the real trajectory and pass through the scatterer. The event line that marks the occurring of scattering event, passes through the center of scatterer and the starting point (red empty dot) on the initial asymptote. The incoming momentum $\mathbf{k}$ and outgoing momentum $\mathbf{k}'$ are defined as the starting (red empty dot) and ending point (blue empty dot) on the initial and final asymptote, respectively.

In contrast, in the presence of magnetic field, the trajectory is bent, and we use the abstraction of the scattering process discussed in the previous subsections to define scattering parameters, as shown in Fig. 3. The incoming momentum $\mathbf{k}$ and outgoing momentum $\mathbf{k}'$ cannot be defined straightforwardly, due to the directions of the initial/final asymptote changes over time. As shown in Fig. 3, the red and blue dashed lines are the asymptotic trajectory which completes the circular trajectory. The incoming $\mathbf{k}$ and outgoing $\mathbf{k}'$ are defined along the tangential direction to the initial asymptote and final asymptote at the starting point and ending point, respectively (see Fig. 3). The $\mathbf{k}$ and $\mathbf{k}'$ are rotated by the same angle in unit time.

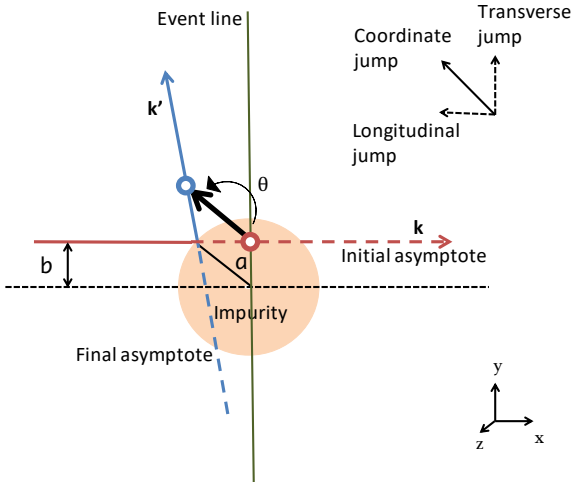

FIG. 2. The illustration of the conventional hard ball scattering with no magnetic field. The red and blue empty dot are the starting point and ending point, respectively. The green line is the event line passing through starting point and impurity center. The initial asymptote and final asymptote are marked by dashed red and blue line with the incoming momentum $\mathbf{k}$, the outgoing momentum $\mathbf{k}'$, and the angle of scattering θ, the impact parameter b. The coordinate jump can be divided into two directions, which are transverse jump and longitudinal jump.

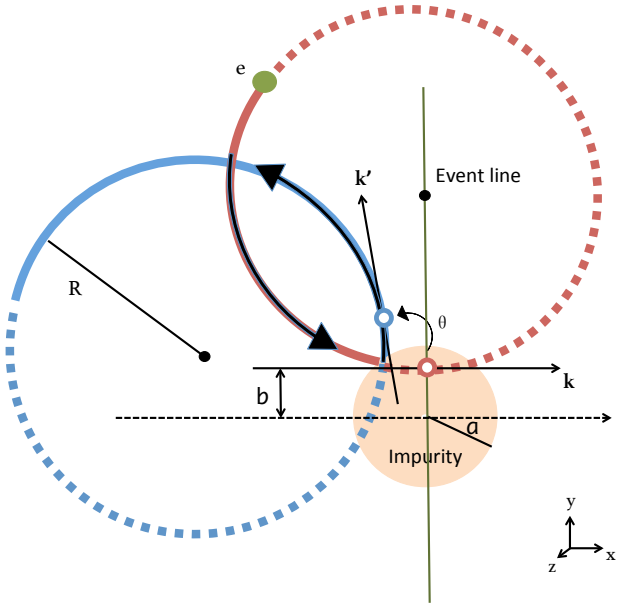

FIG. 3. The illustration of electron scattering on hard disk impurity with cyclotron orbit under magnetic field. The impurity radius is a. The cyclotron radius is R. The red and blue solid lines are the real trajectory of the incoming and outgoing electron, respectively. The red and blue complete circle forms the initial asymptote and final asymptote. The red and blue empty dots are the starting point and ending point, respectively. The incoming momentum $\mathbf{k}$ and the outgoing momentum $\mathbf{k}'$ are along the tangential direction at the starting point and ending point. The angle of scattering θ is the angle between $\mathbf{k}$ and $\mathbf{k}'$.

In the Appendix E, we demonstrate how the abstraction method can be applied to the soft potential under magnetic field.

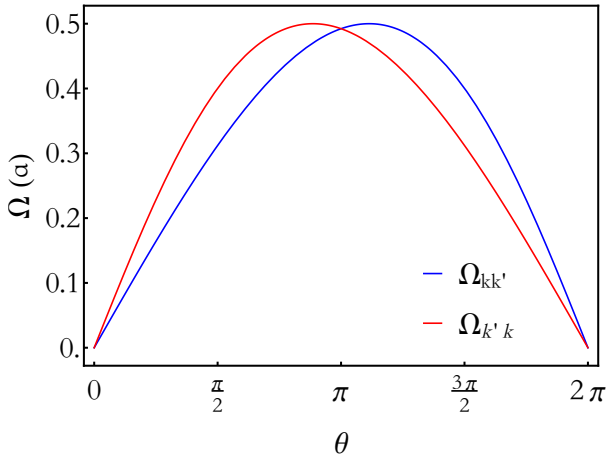

FIG. 4. The plots of the differential cross section of two processes: $\mathbf{k} \to \mathbf{k}'$ and $\mathbf{k}' \to \mathbf{k}$, respectively, in the unit of impurity radius a. The ratio $\frac{a}{R} = 0.16$. The $\Omega_{\mathbf{k}\mathbf{k}'}$ does not overlap with $\Omega_{\mathbf{k}'\mathbf{k}}$, which leads to skew scattering.

C. Skew scattering under magnetic field

In this section, we discuss the skew scattering in the classical picture. As shown in previous literatures, the antisymmetric part of the probability of scattering $W_{\mathbf{k}\mathbf{k}'}$ leads to the skew scattering [10]. $W_{\mathbf{k}\mathbf{k}'}$ (probability of scattering of $\mathbf{k} \to \mathbf{k}'$ process) is related to the differential cross section as $W_{\mathbf{k}\mathbf{k}'} = n_i v_{\mathbf{k}} \Omega_{\mathbf{k}\mathbf{k}'}$, where n_i is the impurity concentration and $v_{\mathbf{k}}$ is the electron velocity. For hard-disk potentials, the scattering is elastic, i.e. $|v_{\mathbf{k}}| = |v_{\mathbf{k}'}|$. Therefore, a nontrivial antisymmetric part of $W_{\mathbf{k}\mathbf{k}'}$ only comes from that $\Omega_{\mathbf{k}\mathbf{k}'} \neq \Omega_{\mathbf{k}'\mathbf{k}}$.

Using the scattering parameters shown in Fig. 3, the differential cross section is easily calculated by $\Omega_{\mathbf{k}\mathbf{k}'} = \left|\frac{db}{d\theta}\right|$. Here we use the fact that b is only a function of θ and $k = |\mathbf{k}|$ due to the rotational symmetry and the elastic nature of scattering. For two-dimensional Lorentz model, the relation between b and θ and k (with $R = \hbar k/(eB)$) is given by (derived in Appendix A)

$$b(\theta, k) = -R + \sqrt{a^2 + R^2 + 2aR\cos\frac{\theta}{2}}, \tag{1}$$

Therefore, the differential cross section reads as

$$\Omega_{\mathbf{k}\mathbf{k}'} = \frac{a\sin\frac{\theta}{2}}{2\sqrt{1 + 2\frac{a}{R}\cos\frac{\theta}{2} + \left(\frac{a}{R}\right)^2}}. \tag{2}$$

On the other hand, the differential cross section of the inverse process $\mathbf{k}' \to \mathbf{k}$ is labeled by $\Omega_{\mathbf{k}'\mathbf{k}}$, and can be calculated as follows: $\Omega_{\mathbf{k}'\mathbf{k}} = \left|\frac{db}{d\theta}\right|_{\theta \to 2\pi - \theta}$. Therefore, its expression reads as

$$\Omega_{\mathbf{k}'\mathbf{k}} = \frac{a\sin\frac{\theta}{2}}{2\sqrt{1 - 2\frac{a}{R}\cos\frac{\theta}{2} + \left(\frac{a}{R}\right)^2}}. \tag{3}$$

We plot $\Omega_{\mathbf{k}\mathbf{k}'}$ and $\Omega_{\mathbf{k}'\mathbf{k}}$ in Fig. 4. It shows that $\Omega_{\mathbf{k}\mathbf{k}'} \neq \Omega_{\mathbf{k}'\mathbf{k}}$, leading to the nontrivial skew scattering contribution to the electron transport in two-dimensional Lorentz model. In Eq. 22 in Section III B and Section IV C, we will find out that only when $\Omega_{\mathbf{k}\mathbf{k}'} \neq \Omega_{\mathbf{k}'\mathbf{k}}$, there is $\frac{1}{\tau^\perp} \neq 0$ ($\frac{1}{\tau^\perp}$ is the reciprocal of transverse relaxation time), which is the signature of skew scattering. We further comment that the nature of the above inequivalence is a finite magnetic field, i.e. only in the limit $\mathbf{B} \to 0$, $R \to \infty$ and hence $\Omega_{\mathbf{k}\mathbf{k}'} - \Omega_{\mathbf{k}'\mathbf{k}} \to 0$. Therefore, a finite magnetic field is essential to the skew scattering mechanism, which breaks the time-reversal symmetry. Moreover, the leading order contribution to $\Omega_{\mathbf{k}\mathbf{k}'} - \Omega_{\mathbf{k}'\mathbf{k}}$ is porportional to $\frac{a}{R}$ as shown in Eq. 22 in Section III B. Therefore, the correction to the Boltzmann transport theory by the skew scattering is relatively small due to the smallness of $\frac{a}{R}$.

D. Coordinate jump under magnetic field

In this section, we discuss the coordinate jump [11, 23, 24], labeled by $\delta\mathbf{r}_{\mathbf{k}'\mathbf{k}}$ (coordinate jump from $\mathbf{k} \to \mathbf{k}'$). In our recipe of describing the impurity scattering, it can be conveniently defined as the difference between the starting point $\mathbf{r}_s$ and the ending point $\mathbf{r}_e$: $\delta\mathbf{r}_{\mathbf{k}'\mathbf{k}} = \mathbf{r}_e - \mathbf{r}_s$. It can be further divided into longitudinal jump and transverse jump, which are parallel and orthogonal to the incoming momentum $\mathbf{k}$, respectively (Fig. 2).

As the incoming momentum is along x-axis, the longitudinal jump is $\delta\mathbf{x}_{\mathbf{k}'\mathbf{k}}$, and the transverse jump is $\delta\mathbf{y}_{\mathbf{k}'\mathbf{k}}$. Similar to the differential cross section, the coordinate jump is also a functions of θ and k, and can be calculated as follows based on the two-dimensional Lorentz model (derived in Appendix B)

$$\delta\mathbf{x}_{\mathbf{k}'\mathbf{k}} = R\left[\sin\theta - \frac{\sin\theta + 2\frac{a}{R}\sin\left(\frac{\theta}{2}\right)}{\sqrt{1 + \frac{2a}{R}\cos(\frac{\theta}{2}) + \frac{a^2}{R^2}}}\right]\hat{\mathbf{x}}, \tag{4}$$

$$\delta\mathbf{y}_{\mathbf{k}'\mathbf{k}} = 2R\sin^2\left(\frac{\theta}{2}\right)\left[1 - \frac{1}{\sqrt{1 + \frac{2a}{R}\cos(\frac{\theta}{2}) + \frac{a^2}{R^2}}}\right]\hat{\mathbf{y}}. \tag{5}$$

Generally, the coordinate jump has two contributions to the electron transport. First, it may induce a net jump velocity $\mathbf{v}_{cj}$ that modifies the electronic drift velocity:

$$\mathbf{v}_{cj} = \sum_{\mathbf{k}'} W_{\mathbf{k}\mathbf{k}'}\delta\mathbf{r}_{\mathbf{k}'\mathbf{k}} = \int_0^{2\pi} d\theta n_i v \Omega_{\mathbf{k}\mathbf{k}'}\delta\mathbf{r}_{\mathbf{k}'\mathbf{k}}, \tag{6}$$

with $v = \hbar k/m$. Secondly, it leads to an electrostatic potential difference $e\mathbf{E}\cdot\delta\mathbf{r}_{\mathbf{k}'\mathbf{k}}$ and thus affects the electronic equilibrium distribution function.

As will be seen from Eq. 26-31 of Section III B, the side jump can be expanded as a power series with respect to $\frac{a}{R}$. Due to the smallness of $\frac{a}{R}$, the side jump correction to the Drude theory is relatively small.

Finally, we comment that as $\mathbf{B} \to 0$ the transverse jump does not have a net jump velocity, as the system respects a mirror symmetry with the mirror passing through the scatterer, parallel to $\mathbf{k}$, and normal to the material plane. On the other hand, the longitudinal jump is not restricted by any symmetry and hence the net jump velocity is nonzero. Both statements can be easily verified for the two-dimensional Lorentz model using Eq. 2, 4, 5 and 6.

E. The nature of the anisotropic scattering

In the first glance, the assignment of the scattering events of $t = 0$ at the event line instead of the circular boundary of scatter is counterintuitive and artificial. However, it has deeper physical ground underneath.

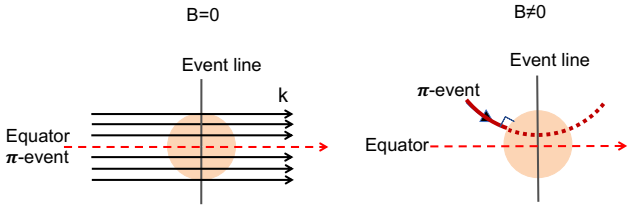

FIG. 5. The illustration of 'π event' (when the scattering angle is π) in the absence and presence of magnetic field.

The advantage of using the event line defined in our theory instead of the colliding boundary, is that the cross sectional area (which overlaps with the event line) is the projection of the boundary. The incoming scattering events are uniformly distributed on the event line with momentum perpendicular to the event line, but not uniform on the boundary. Therefore, the number of electrons being scattered is proportional to the cross-sectional area on the event line. This provides convenience to count the number of scattering events and scattering cross section.

In order to understand the nature of anisotropic scattering, we define 'π event' as the scattering event with scattering angle $\theta = \pi$. When there is no magnetic field, the 'π event' evenly divides the cross sectional area along the event line (Fig. 5) and there is no skew scattering. When there is magnetic field present, the π event unevenly divides the cross-sectional area on the event line (Fig. 5), resulting in the uneven division of the number of electrons being scattered up (with the scattering angle within $[0, \pi]$) and scattered down (with the scattering angle within $[\pi, 2\pi]$). This is shown in Fig. 6, where the red shaded area (corresponding to the cross-sectional area being scattered up) is smaller than the green shaded area (corresponding to the cross-sectional area being scattered down).

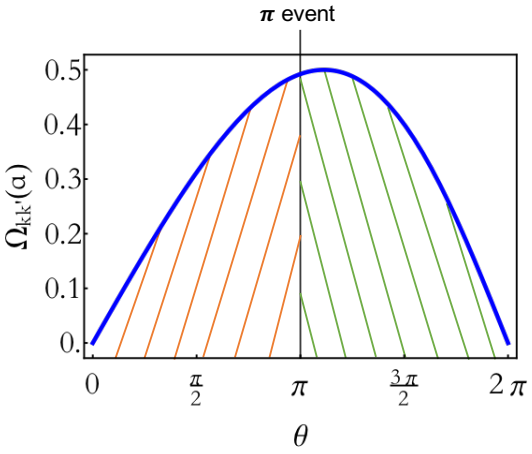

FIG. 6. The plot of differential cross section of $\mathbf{k} \to \mathbf{k}'$ process in the unit of impurity radius a. The vertical black line marks the π event. The red shaded area is the cross sectional area within scattering angle $[0, \pi]$. The green shaded area is the cross sectional area within scattering angle $[\pi, 2\pi]$. The π-event unevenly divides the cross sectional area, with the red shaded area smaller than the green shaded area.

We provide a second way to understand the anisotropic scattering in Appendix F.

F. Modified Boltzmann equation

The Boltzmann equation can be generalized to include the skew scattering and coordinate jump, reading as ($e > 0$)

$$(-e)\left(\mathbf{E} + \mathbf{v} \times \mathbf{B}\right) \cdot \frac{\partial f_{\mathbf{k}}}{\hbar \partial \mathbf{k}} = -n_i v \int_0^{2\pi} d\theta \left[\Omega_{\mathbf{k}\mathbf{k}'} f\left(\epsilon, \mathbf{k}\right) - \Omega_{\mathbf{k}'\mathbf{k}} f\left(\epsilon, \mathbf{k}'\right) + \Omega_{\mathbf{k}'\mathbf{k}} \partial_\epsilon f^0 e\mathbf{E} \cdot \delta \mathbf{r}_{\mathbf{k}'\mathbf{k}}\right], \tag{7}$$

where f^0 is the equilibrium distribution function. We emphasize that in the above equation, $|\mathbf{k}'| = |\mathbf{k}|$ because the scattering is elastic.

To solve up to the linear order of electric field, we assume that

$$f\left(\epsilon, \mathbf{k}\right) = f^0\left(\epsilon\right) + g^{\mathrm{r}}\left(\epsilon, \mathbf{k}\right) + g^{\mathrm{cj}}\left(\epsilon, \mathbf{k}\right), \tag{8}$$

where $g^{\mathrm{cj}}\left(\epsilon, \mathbf{k}\right)$ is the part of the non-equilibrium distri-

bution function purely due to the coordinate jump (or called anomalous distribution function), and $g^{\rm r}$ is the non-equilibrium distribution function in the absence of coordinate jump (or called normal distribution function). Combining Eq. 7 and Eq. 8, keeping the terms of linear order in the electric and magnetic field, and ignoring the coupling between skew scattering and coordinate jump, the Boltzmann equation is decomposed into two equations:

$$(-e)\,\mathbf{E}\cdot\frac{\partial f^0}{\hbar\partial\mathbf{k}}+(-e)\,(\mathbf{v}\times\mathbf{B})\cdot\frac{\partial g^{\rm r}_{\mathbf{k}}}{\hbar\partial\mathbf{k}}=-\int_0^{2\pi}d\theta n_i v\left[\Omega_{\mathbf{k}\mathbf{k}'}g^{\rm r}_{\mathbf{k}}-\Omega_{\mathbf{k}'\mathbf{k}}g^{\rm r}_{\mathbf{k}'}\right], \tag{9}$$

$$(-e)\,\mathbf{E}\cdot\left(\int_0^{2\pi}d\theta n_i v\Omega_{\mathbf{k}'\mathbf{k}}\delta\mathbf{r}_{\mathbf{k}'\mathbf{k}}\right)\partial_\epsilon f^0-(-e)\,(\mathbf{v}\times\mathbf{B})\cdot\frac{\partial g^{\rm cj}_{\mathbf{k}}}{\hbar\partial\mathbf{k}}=\int_0^{2\pi}d\theta n_i v\left[\Omega_{\mathbf{k}\mathbf{k}'}g^{\rm cj}_{\mathbf{k}}-\Omega_{\mathbf{k}'\mathbf{k}}g^{\rm cj}_{\mathbf{k}'}\right]. \tag{10}$$

With all the above ingredients the electrical current density is given by

$$\mathbf{j}=(-e)\int\frac{d\mathbf{k}}{4\pi^2}\left[g^{\rm r}+g^{\rm cj}\right]\left[\mathbf{v}+\mathbf{v}^{cj}\right]. \tag{11}$$

III. SOLUTIONS OF THE BOLTZMANN EQUATION

A. Zero magnetic field case

In this case, only the longitudinal coordinate jump along the $\mathbf{k}$-direction exists. $\mathbf{v}^{cj}\equiv\int_0^{2\pi}d\theta n_i v\Omega(\theta)\,\delta\mathbf{r}_{\mathbf{k}'\mathbf{k}}=-\mathbf{v}\frac{3\pi n_i a^2}{4}$ which is along the opposite direction to $\mathbf{v}$.

The Boltzmann equation is solved as

$$g^{\rm r}_{\mathbf{k}}=\left(-\partial_\epsilon f^0\right)(-e)\,\mathbf{E}\cdot\mathbf{v}\tau^0(\epsilon), \tag{12}$$

$$g^{\rm cj}_{\mathbf{k}}=\left(\partial_\epsilon f^0\right)(-e)\,\mathbf{E}\cdot\mathbf{v}^{cj}\tau^0(\epsilon), \tag{13}$$

where $\frac{1}{\tau^0(\epsilon)}=n_i v\frac{8a}{3}$. The electric current density is therefore $j_x\equiv\left(\sigma^0+\sigma^{cj1}+\sigma^{cj2}+\sigma^{cj1,cj2}\right)E_x$ with

$$\sigma^0=(-e)\sum_k\frac{g^{\rm r}_{\mathbf{k}}}{E_x}v_x=\frac{ne^2\tau^0(\epsilon_F)}{m}, \tag{14}$$

$$\sigma^{\rm cj1}=(-e)\sum_k\frac{g^{\rm cj}_{\mathbf{k}}}{E_x}v_x=\frac{3n_i\pi a^2}{4}\frac{ne^2\tau^0(\epsilon_F)}{m}, \tag{15}$$

$$\sigma^{\rm cj2}=(-e)\sum_k\frac{g^{\rm r}_{\mathbf{k}}}{E_x}v^{\rm cj}_x=-\sigma^{\rm cj1}, \tag{16}$$

and

$$\sigma^{\rm cj1,cj2}=(-e)\sum_k\frac{g^{\rm cj}_{\mathbf{k}}}{E_x}v^{\rm cj}_x=-\frac{ne^2\tau^0(\epsilon_F)}{m}\left(\frac{3n_i\pi a^2}{4}\right)^2, \tag{17}$$

where the carrier density $n=\frac{m\epsilon_F}{\pi\hbar^2}$ with ϵ_F the Fermi energy.

Here, σ^0 is the conventional zero-field conductivity in the Drude theory. $\sigma^{\rm cj1}$ is the conductivity induced by the anomalous distribution from the coordinate jump. $\sigma^{\rm cj2}$ is the conductivity induced by the velocity correction from the coordinate jump. It cancels $\sigma^{\rm cj1}$. $\sigma^{\rm cj1,cj2}$ is the conductivity with both the distribution and velocity being corrected by the coordinate jump. Therefore, the total electrical conductivity is

$$\sigma=\sigma^0+\sigma^{\rm cj1,cj2}=\frac{ne^2\tau^0(\epsilon_F)}{m}\left[1-\left(\frac{3}{4}n_i\pi a^2\right)^2\right]. \tag{18}$$

There is a correction to the electron density, because the electrons are only present in the free area excluding the area occupied by impurities. The electron density $n=\frac{N}{A-A_i}=\frac{n_D}{1-\frac{A_i}{A}}$, where A and A_i represent the total 2D area and the area occupied by the hard disk impurities, respectively, and $\frac{A_i}{A}=\pi n_i a^2$, and $n_D=\frac{N}{A}$ is the electron density without the correction to exclude the area that impurities take. Thus, the Fermi momentum $k_F=\sqrt{2\pi n}=\frac{{k_F}^D}{\sqrt{1-\frac{A_i}{A}}}$, where $k_F^D=\sqrt{2\pi n_D}$.

Therefore, the measured electrical conductivity is also corrected by

$$\begin{aligned}\sigma^M&=\sigma\frac{A-A_i}{A}\\&=\frac{n_De^2\tau^D}{m}\left[1-\left(\frac{3}{4}\pi n_i a^2\right)^2\right]\sqrt{1-\pi n_i a^2},\end{aligned} \tag{19}$$

with the Drude transport relaxation rate $1/\tau^D=n_i v_F^D\frac{8a}{3}$ a constant. The conductivity in our theory σ^M is lower than the Drude conductivity $\sigma^D=\frac{n_De^2\tau^D}{m}$ by a factor of $\left[1-\left(\frac{3}{4}\pi n_i a^2\right)^2\right]\sqrt{1-\pi n_i a^2}$ as can be seen from Eq. 19, which decreases as a function of the dimensionless quantity $n_i a^2$. The deviation of the diffusion coefficient from the Drude model in a previous computer simulation of Lorentz model with overlapped hard sphere impurities [12] is similar to that in our theory.

B. Low magnetic field case: Hall coefficient and magnetoresistivity

In this section, we evaluate the conductivity under a weak magnetic field. We first discuss the contribution from the skew scattering. According to previous discussions, we need to solve the distribution function using Eq. 9.

$g^{\mathrm{r}}_{\mathbf{k}} = \left(-\partial_\epsilon f^0\right)(-e)\left[\mathbf{E}\cdot\mathbf{v}\tau^L(\epsilon) + (\hat{\mathbf{z}}\times\mathbf{E})\cdot\mathbf{v}\tau^T(\epsilon)\right]$ into Eq. 9 and obtain

$$\tau^L(\epsilon) = \frac{\tau^{\parallel}(\epsilon)}{1+\left[\omega_c\tau^{\parallel}(\epsilon)+\frac{\tau^{\parallel}(\epsilon)}{\tau^{\perp}(\epsilon)}\right]^2},$$
$$\tau^T(\epsilon) = \left[\omega_c\tau^{\parallel}(\epsilon)+\frac{\tau^{\parallel}(\epsilon)}{\tau^{\perp}(\epsilon)}\right]\tau^L(\epsilon), \tag{20}$$

where we define

$$\frac{1}{\tau^{\parallel}(\epsilon)} = \int_0^{2\pi} d\theta n_i v[\Omega^A(1+\cos(\theta))+\Omega^S(1-\cos(\theta))] = \frac{8}{3}n_i v a\left[1-\frac{1}{5}\left(\frac{a}{R}\right)^2+O\left(\left(\frac{a}{R}\right)^4\right)\right], \tag{21}$$

$$\frac{1}{\tau^{\perp}(\epsilon)} = \int_0^{2\pi} d\theta n_i v[\Omega^S-\Omega^A]\sin(\theta) = -\frac{\pi}{4}n_i v a\frac{a}{R}\left[1+O\left(\left(\frac{a}{R}\right)^2\right)\right]. \tag{22}$$

Here $\Omega^A = \frac{1}{2}(\Omega_{\mathbf{kk'}}-\Omega_{\mathbf{k'k}})$, which is the antisymmetric part of the differential cross section, and $\Omega^S = \frac{1}{2}(\Omega_{\mathbf{k'k}}+\Omega_{\mathbf{kk'}})$, which is the symmetric part of the differential cross section. $\tau^{\perp}$ is purely due to the skew scattering, i.e. $\Omega_{\mathbf{kk'}} \neq \Omega_{\mathbf{k'k}}$. In our theory, only when $B \neq 0$, $\Omega_{\mathbf{kk'}} \neq \Omega_{\mathbf{k'k}}$.

Generally, we prove that $\tau^{\parallel}$ is purely contributed by Ω^S by showing $\int_0^{2\pi} d\theta\Omega^A(1+\cos(\theta)) = 0$, and $\tau^{\perp}$ is purely contributed by Ω^A by showing $\int_0^{2\pi} d\theta\Omega^S\sin(\theta) = 0$ (see Appendix D). As a result, $\tau^{\parallel}$ is not enough to characterize the collision process as long as the scattering probability contains an antisymmetric part, in which case, $\tau^{\perp}$ naturally emerges.

In our example, $\frac{1}{\tau^{\perp}}$ is always negative (as shown in Eq. 22 and Fig. 7). Moreover, the ratio of $\tau^{\parallel}$ to $\tau^{\perp}$ is proportional to a/R. Since we are considering the weak magnetic field scenario with a large R ($R > a$), $|\tau^{\perp}|$ will be bigger than $|\tau^{\parallel}|$. Taking the data from the second row of Table I as example where $\beta = 0.6$, $\frac{a}{R} = \frac{2\beta c}{\pi} = 0.06$, the ratio of $\tau^{\parallel}$ to $\tau^{\perp}$ is then around -0.017.

The finite magnetoresistance in our theory is crucially provided by the finite impurity size a. As Eq. 22 shows, $\frac{1}{\tau^{\perp}}$ exists only when $\frac{a}{R}$ is finite. As Eq. 21 shows, $\frac{1}{\tau^{\parallel}}$ deviates from Drude model, only when $\frac{a}{R}$ is finite. Generally speaking, it also indicates that longer range scatterers leads to a more significant deviation from Drude model at low magnetic fields. This phenomenon is consistent with literature [15] emphasizing that the classical magnetoresistance is crucially affected by long-range disorder. We will explore more about the long-range disorder case in Appendix E.

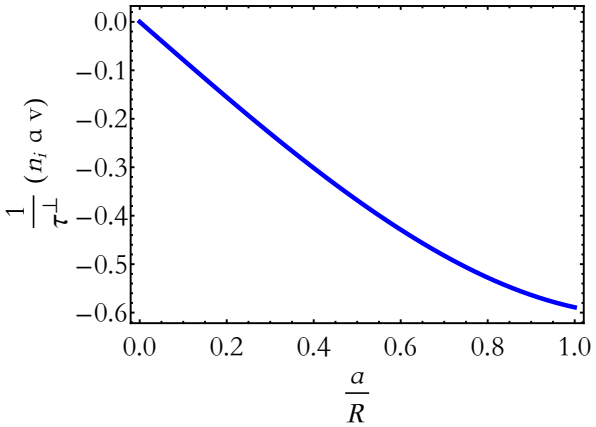

FIG. 7. The plot of the reciprocal of transverse relaxation time $\frac{1}{\tau^{\perp}}$ in the unit of $n_i a v$, where a is the impurity radius, n_i is the impurity density, and v is the electron velocity. The $\frac{1}{\tau^{\perp}}$ is always negative as long as $a < R$.

The conductivity resulted from the skew scattering is

$$\begin{bmatrix}\sigma_{xx}\\ \sigma_{yx}\end{bmatrix} = \frac{\frac{ne^2\tau^{\parallel}}{m}}{1+\left(\omega_c\tau^{\parallel}+\frac{\tau^{\parallel}}{\tau^{\perp}}\right)^2}\begin{bmatrix}1\\ (eB+\frac{m}{\tau^{\perp}})\frac{\tau^{\parallel}}{m}\end{bmatrix}. \tag{23}$$

Converting the conductivity in Eq. 23 into resistivity, we get

$$\rho_{xx} = \frac{m}{e^2\tau^{\parallel}n}, \tag{24}$$

$$\rho_{xy} = -\left(\frac{B}{en} + \frac{m}{e^2\tau^{\perp}n}\right). \tag{25}$$

where $\frac{1}{\tau^{\parallel}}$ and $\frac{1}{\tau^{\perp}}$ was derived in Eq. 21 and Eq. 22, respectively.

As Eq. 24 and Eq. 25 shows, $\tau^{\parallel}$ contributes to the negative magnetoresistance, while $\tau^{\perp}$ contributes to the anomalous Hall effect. The $\frac{1}{\tau^{\parallel}}$ decreases with the increase of magnetic field, which results in the negative magnetoresistance. We will explore more of $\tau^{\perp}$ from Drude theory perspective in Section IV Discussion, part C.

We now discuss the contribution from coordinate jump to the conductivity. For the anomalous distribution function due to coordinate jump, we first calculate

$$\int_0^{2\pi} d\theta n_i v \Omega_{\mathbf{k}'\mathbf{k}} \delta\mathbf{r}_{\mathbf{k}'\mathbf{k}} = n_i a^2 \left(C_a^{\parallel}\mathbf{v} + C_a^{\perp}\hat{\mathbf{z}}\times\mathbf{v}\right), \tag{26}$$

and

$$\int_0^{2\pi} d\theta n_i v \Omega_{\mathbf{k}\mathbf{k}'} \delta\mathbf{r}_{\mathbf{k}'\mathbf{k}} = n_i a^2 \left(C_{cj}^{\parallel}\mathbf{v} + C_{cj}^{\perp}\hat{\mathbf{z}}\times\mathbf{v}\right), \tag{27}$$

where

$$C_a^{\parallel} \equiv -\tfrac{3}{4}\pi + \tfrac{7\pi}{16}\left(\tfrac{a}{R}\right)^2 + O\left(\tfrac{a}{R}\right)^4, \tag{28}$$

$$C_a^{\perp} \equiv \frac{16}{15}\frac{a}{R} + \frac{88}{105}\left(\frac{a}{R}\right)^3 + O\left(\frac{a}{R}\right)^5, \tag{29}$$

$$C_{cj}^{\parallel} \equiv -\tfrac{3}{4}\pi + \tfrac{\pi}{16}\left(\tfrac{a}{R}\right)^2 + O\left(\tfrac{a}{R}\right)^4, \tag{30}$$

$$C_{cj}^{\perp} \equiv \frac{8}{105}\left(\frac{a}{R}\right)^3 + O\left(\frac{a}{R}\right)^5. \tag{31}$$

Then we plug the following ansatz

$$g_{\mathbf{k}}^{\mathrm{cj}} = \left(-\partial_\epsilon f^0\right)(-e)\, n_i a^2 \left[\mathbf{E}\cdot\mathbf{v}\tau^{L,\mathrm{cj}}(\epsilon) + (\hat{\mathbf{z}}\times\mathbf{E})\cdot\mathbf{v}\tau^{T,\mathrm{cj}}(\epsilon)\right], \tag{32}$$

into Eq. 10 and get

$$\tau^{L,cj}(\epsilon) = \frac{-C_a^{\parallel} - C_a^{\perp}\left[\omega_c\tau^{\parallel}(\epsilon) + \frac{\tau^{\parallel}(\epsilon)}{\tau^{\perp}(\epsilon)}\right]}{1 + \left(\omega_c\tau^{\parallel}(\epsilon) + \frac{\tau^{\parallel}(\epsilon)}{\tau^{\perp}(\epsilon)}\right)^2}\tau^{\parallel}(\epsilon), \tag{33}$$

$$\tau^{T,cj}(\epsilon) = \frac{C_a^{\perp} - C_a^{\parallel}\left(\omega_c\tau^{\parallel}(\epsilon) + \frac{\tau^{\parallel}(\epsilon)}{\tau^{\perp}(\epsilon)}\right)}{1 + \left(\omega_c\tau^{\parallel}(\epsilon) + \frac{\tau^{\parallel}(\epsilon)}{\tau^{\perp}(\epsilon)}\right)^2}\tau^{\parallel}(\epsilon). \tag{34}$$

Combining the skew scattering and coordinate jump contributions to the conductivity, we obtain the following result

$$\sigma_{||} \equiv \frac{j_x}{E_x} = \sigma_{xx}\left(1 + \tan^2\theta_H\right), \tag{35}$$

$$R_H(\epsilon_F, B) \equiv \frac{E_y}{j_x B} = -\frac{1}{B}\frac{\tan\theta_H}{\sigma_{xx}\left(1+\tan^2\theta_H\right)}, \tag{36}$$

where $\tan\theta_H \equiv \frac{\sigma_{yx}}{\sigma_{xx}}$ denotes the Hall angle, and the Hall coefficient R_H depends on the magnetic field and ϵ_F. Usually only the magnetic field-independent Hall coefficient $R_H|_{B=0}$ is needed. The magnetoresistivity is $\frac{\delta\rho_{xx}(B)}{\rho_{xx}(B=0)} = -\frac{\delta\sigma_{xx}(B)}{\sigma_{xx}(B=0)}$ where $\rho_{xx} = \sigma_{xx}^{-1}$ is the resistivity and $\delta\sigma_{xx}(B) \equiv \sigma_{xx}(B) - \sigma_{||}(B=0)$ is the magnetoconductivity. Because

$$\begin{bmatrix}\sigma_{xx}\\ \sigma_{yx}\end{bmatrix} = \frac{e^2\epsilon_F}{\pi\hbar^2}\begin{bmatrix}1+n_ia^2C_{cj}^{\parallel} & -n_ia^2C_{cj}^{\perp}\\ n_ia^2C_{cj}^{\perp} & 1+n_ia^2C_{cj}^{\parallel}\end{bmatrix}\begin{bmatrix}\tau^L + n_ia^2\tau^{L,cj}\\ \tau^T + n_ia^2\tau^{T,cj}\end{bmatrix}. \tag{37}$$

In the case of $n_ia^2 \ll 1$ and $\omega_c\tau^0 < 1$, we can neglect $C_{cj}^{\perp}$ and obtain

$$\begin{bmatrix}\sigma_{xx}\\ \sigma_{yx}\end{bmatrix} = \frac{ne^2}{m}\frac{\left(1+n_ia^2C_{cj}^{\parallel}\right)\tau^{\parallel}}{1+\left(\omega_c\tau^{\parallel}+\frac{\tau^{\parallel}}{\tau^{\perp}}\right)^2}\begin{bmatrix}1+n_ia^2\left[-C_a^{\parallel} - C_a^{\perp}\left(\omega_c\tau^{\parallel}+\frac{\tau^{\parallel}}{\tau^{\perp}}\right)\right]\\ \left(\omega_c\tau^{\parallel}+\frac{\tau^{\parallel}}{\tau^{\perp}}\right) + n_ia^2\left[C_a^{\perp} - C_a^{\parallel}\left(\omega_c\tau^{\parallel}+\frac{\tau^{\parallel}}{\tau^{\perp}}\right)\right]\end{bmatrix}. \tag{38}$$

This is the complete expression of the conductivity including the skew scattering and coordinate jump effect. Then we can solve for the Hall coefficient and the magnetoresistivity.

The full expression of Hall angle is given by

$$\tan\theta_H = \frac{\left(\omega_c\tau^{\parallel}+\frac{\tau^{\parallel}}{\tau^{\perp}}\right) + n_ia^2\left[C_a^{\perp} - C_a^{\parallel}\left(\omega_c\tau^{\parallel}+\frac{\tau^{\parallel}}{\tau^{\perp}}\right)\right]}{1 + n_ia^2\left[-C_a^{\parallel} - C_a^{\perp}\left(\omega_c\tau^{\parallel}+\frac{\tau^{\parallel}}{\tau^{\perp}}\right)\right]}. \tag{39}$$

To expand the Hall coefficient and the magnetoresistivity, we use the approximation $n_i a^2 \ll 1$. The Hall angle and the magnetoconductivity are

$$\tan\theta_H \simeq \omega_c\tau^0\left[1-\frac{\pi}{4}n_i a^2+\frac{128}{45}\left(n_i a^2\right)^2\right], \tag{40}$$

and

$$\frac{\sigma_{||}(B)-\sigma_{||}(0)}{\sigma_{||}(0)} \simeq \frac{64}{15}\left(n_i a^2\omega_c\tau^0\right)^2=\frac{3}{5}\left(\frac{a}{R}\right)^2>0, \tag{41}$$

respectively. The correction due to the effective area of free space excluding the area of all the impurities is of higher order and thus neglected.

The magnetoresistivity $\frac{\delta\rho_{\parallel}(B)}{\rho_{\parallel}(0)} \simeq -\frac{64}{15}\left(n_i a^2\omega_c\tau^0\right)^2$ is negative, and is composed of three contributions: 1) the contribution from the Hall angle, more specifically, from the anomalous distribution function to the Hall transport $\left(C_a^{\perp}\to\tau^{T,cj}\to\tan\theta_H\right)$; 2) the magnetic-field-induced correction to the longitudinal transport relaxation time $\left(\left(\tau^{\parallel}-\tau^0\right)\to\sigma_{xx}\right)$; 3) the contribution of anomalous distribution function to the longitudinal transport $\left(C_a^{\perp}\to\tau^{L,cj}\to\sigma_{xx}\right)$.

The leading order correction of the Hall angle $-\frac{\pi}{4}n_i a^2\omega_c\tau^0$ stems from the magnetic-field-induced skew scattering. This result is comparable to the Hall angle from the classical memory effect [8] in the limit $n_i a^2 \ll \omega_c\tau_D \ll 1$: $\delta R_H^{cm}/R_H^B = -\frac{32}{9\pi}n_i a^2$, where R_H^B is the Hall coefficient in the conventional Boltzmann theory $R_H^B = -\frac{1}{n_D e} = -\frac{1}{ne(1-\pi n_i a^2)}$, and δR_H^{cm} is the difference between the Hall coefficient corrected by classical memory effect and the conventional Hall coefficient.

In experiments, to obtain the real electron density n from the measured Hall coefficient, the correction to R_H has to be included. The Hall coefficient is $R_H = -1/n'e$, where n' is the effective electron density $n' \approx \frac{n}{\left(1-\frac{c}{4}+\frac{128c^2}{45\pi^2}\right)}$ and $c=\pi a^2 n_i$. We use the value of $c=0.15$ here as an example (this value is also used in the discussion) and find that $n' \approx \frac{n}{0.97}$ which is equivalent to a 3% error. This error is larger when the impurity density increases.

We note that in a previous work [25], it is already recognized that there may be corrections to the Hall coefficient. However, their result is due to the magnetic-field-affected Bloch-electron drifting motion, and is proportional to the $\frac{1}{(\tau^0)^2}$ (or equivalently, $(n_i a^2)^2$). In comparison, our correction here has different origins (magnetic-field-affected electron-impurity scattering), as well as different scaling behavior (i.e. proportional to $n_i a^2$).

IV. DISCUSSIONS

A. Magnetoresistivity in comparison with simulation at low magnetic field

In this section, we demonstrate that our theory, together with the memory effect discussed in literatures [6, 7], can yield a better understanding of the numerical simulation of the electron transport in the Lorentz model [6]. At low magnetic field $\omega_c\tau^0 < 1$, the literatures [6, 7] predicted a negative magnetoresistivity due to the influence of magnetic field on the Corridor effect (enhancing the backscattering from the first impurity to the second impurity and back to the first impurity) and on multiple scatterings.

In Table I, we compare the numerical simulation of the electron transport with our theory as well as the memory effect. The relevant parameters are defined as follows: $c=\pi n_i a^2=0.15$, $\beta=\omega_c\tau=\frac{4}{3}\omega_c\tau^0$, where $\tau=(2vn_i a)^{-1}$ is the single-particle scattering time. The second column $\left(\frac{\delta\rho_{\parallel}}{c\rho_0}\right)^{an}=-\frac{12}{5\pi^2}c\beta^2$, which can be obtained from Eq. 41 in our theory. The third column is calculated based on the expression $\frac{\delta\rho'_{\parallel}}{c\rho_0}=-\frac{0.4}{\pi}\beta^2$, which is the quadratic contribution due to the influence of magnetic field on multiple scatterings in [7]. The fourth column $\left(\frac{\delta\rho_{\parallel}^{Cor}}{c\rho_0}\right)^{th}$ is calculated based on the analytical expression of magnetoresistivity due to the Corridor effect in [7]. The fifth column is the summation of all the analytical results from [7]. The sixth column includes our results in addition to the previous analytical results in the fifth column. The seventh column $\left(\frac{\delta\rho_{\parallel}}{c\rho_0}\right)^{si}$ is the simulation result of magnetoresistivity in [6].

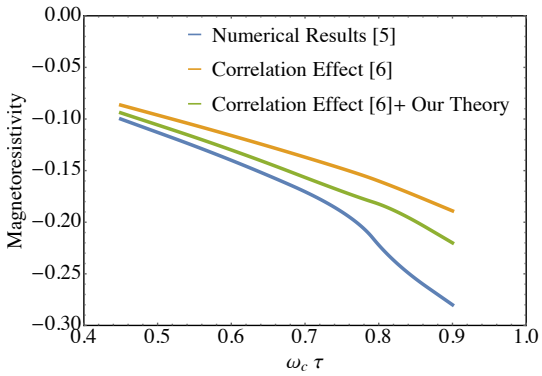

FIG. 8. The plots of the numerical magnetoresistivity in the seventh column of Table 1, the magnetoresistivity from corridor effect in the fourth column of Table 1, and the addition of our magnetoresistivity in the second column of Table 1 with the result from corridor effect, respectively.

As can be seen from table I, the inclusion of $\left(\frac{\delta\rho_{\parallel}}{c\rho_0}\right)^{an}$ (the magnetoresistivity calculated in our theory) yields a more accurate magnetoresistivity, closer to the simu-

β	$\left(\frac{\delta\rho_\parallel}{c\rho_0}\right)^{an}$	$\frac{\delta\rho'_\parallel}{c\rho_0}$	$\left(\frac{\delta\rho^{Cor}_\parallel}{c\rho_0}\right)^{th}$	$\frac{\delta\rho'_\parallel}{c\rho_0}+\left(\frac{\delta\rho^{Cor}_\parallel}{c\rho_0}\right)^{th}$	$\left(\frac{\delta\rho_\parallel}{c\rho_0}\right)^{an}+\frac{\delta\rho'_\parallel}{c\rho_0}+\left(\frac{\delta\rho^{Cor}_\parallel}{c\rho_0}\right)^{th}$	$\left(\frac{\delta\rho_\parallel}{c\rho_0}\right)^{si}$
$\beta/c=3,\beta=0.45$	-0.0074	-0.026	-0.0605	-0.0865	-0.094	-0.1
$\beta/c=4,\beta=0.6$	-0.013	-0.046	-0.07	-0.116	-0.13	-0.14
$\beta/c=5,\beta=0.75$	-0.021	-0.072	-0.076	-0.148	-0.17	-0.19
$\beta/c=5.5,\beta=0.825$	-0.025	-0.087	-0.0796	-0.167	-0.19	-0.24
$\beta/c=6,\beta=0.9$	-0.03	-0.103	-0.086	-0.189	-0.22	-0.28

TABLE I. The comparison between the summation of analytical results from [7] and our theory, and the numerical results from [6]. The second column is calculated based on $\left(\frac{\delta\rho_\parallel}{c\rho_0}\right)^{an}$ is the magnetoresistivity calculated by our formula. The third column $\frac{\delta\rho'_\parallel}{c\rho_0}$ is the quadratic contribution due to the influences of magnetic field on returns after multiple scatterings in [7]. The fourth column $\left(\frac{\delta\rho^{Cor}_\parallel}{c\rho_0}\right)^{th}$ is the analytical values of magnetoresistivity influenced by Corridor effect in [7]. The fifth column is the summation of all the analytical results from [7]. The sixth column includes our results, in addition to the previous analytical results in the fifth column. The seventh column $\left(\frac{\delta\rho_\parallel}{c\rho_0}\right)^{si}$ is the simulation result of magnetoresistivity in [6].

lation result, especially under relatively small magnetic field ($\beta = 0.45$ and $\beta = 0.6$). This is also reflected in Fig. 8. Under relatively large magnetic field, the deviation of the analytical values from the simulation values increases. We comment that both our theory and the corridor effect in literature [6, 7] gradually become less accurate when β increases. Therefore, at large β, the current theory may not be accurate.

We choose the value of $c = \pi n_i a^2 = 0.15$ in table I because we want to compare with the result from literatures [6, 7] where the largest value of c is 0.15. We choose a larger value of c because the larger c is, the more significant the negative magnetoresistivity effect in our theory. The reason can be found from the expression $\left(\delta\rho_\parallel\right)^{an}/\delta\rho'_\parallel = 6n_i a^2$. As can be seen from Table I, the weight of our theory (column 2) in the total theoretical magnetoresistivity (column 6) increases from 8% to 14%, showing a growing importance of our theory when increasing magnetic field.

B. Magnetoresistivity in comparison with experimental results

In this subsection we discuss the possible relevance of our result to experiments. The negative parabolic magnetoresistivity has been observed in a corrugated 2DEG in GaAs wells [27]. Although the authors explained their observation using the Corridor effect, the fitting value for $n_i a^2$ is far beyond its valid range (in literature [7], the fitting of correlation effect to the experiment has suggested a parameter $n_i a^2 = 2.6$, while its theory of the corridor effect requires $n_i a^2 \ll 1$). Thus, the magnetoresistivity theory in terms of corridor effect in the 2D Lorentz model may not provide a suitable description for the experiments with low magnetic field. In comparison, if we fit the experimental parabolic negative magnetoresistivity in low magnetic field to our formula, we get a reasonable value $n_i a^2 = 0.12$, which may provide a second view point to theoretically interpret the experiment. Noted that our theory is not quantitatively accurate once the deviations from the Drude's behavior become significant, while the magnitude of the quadratic magnetoresistance is around 1% (Fig. 2b in literature [27]), which is indeed a weak deviation from the Drude theory.

At high magnetic field regime, several classical theories and experiments address magnetoresistance behaviors deviating from the Drude's behavior. For example, in literature [17, 18], the magnetic field and temperature dependent magnetoresistance at high magnetic field is explained by the classical theory of suppression of the chaotic dynamics in smooth disordered potentials [19, 20].

We also comment that in some cases, the electron motion is quasi-two-dimensional, and the vertical motion is not negligible. One example is shown in literature [21], in which an in-plane magnetic field is applied and the periodically distributed large-scale impurities are prepared. This is, however, beyond the scope of our theory.

C. Phenomenological inclusion of skew scattering into the Drude model

In this subsection we demonstrate that the skew scattering, signified by $\frac{1}{\tau^\perp}$, can be phenomenologically included into Drude framework using a tensor $\overleftrightarrow{\frac{1}{\tau}}$.

In traditional Drude theory, the scattering rate $\frac{1}{\tau}$ is treated as a scalar. The equation of motion is

$$m\dot{\mathbf{v}} = -e(\mathbf{E} + \mathbf{v}\times\mathbf{B}) - \frac{m\mathbf{v}}{\tau}. \tag{42}$$

In the presence of out of plane magnetic field, due to the rotational symmetry in the two dimensional plane, $\frac{1}{\tau}$ becomes an antisymmetric tensor [10, 23, 29] with

nonzero off-diagonal element:

$$\overleftrightarrow{\frac{1}{\tau}} = \begin{pmatrix} \frac{1}{\tau^{\parallel}} & \frac{1}{\tau^{\perp}} \\ -\frac{1}{\tau^{\perp}} & \frac{1}{\tau^{\parallel}} \end{pmatrix}. \tag{43}$$

The modified equation of motion is

$$m\dot{\mathbf{v}} = -e\begin{pmatrix} E_x \\ E_y \end{pmatrix} - e\begin{pmatrix} v_y B_z \\ -v_x B_z \end{pmatrix} - m\begin{pmatrix} \frac{1}{\tau^{\parallel}} & \frac{1}{\tau^{\perp}} \\ -\frac{1}{\tau^{\perp}} & \frac{1}{\tau^{\parallel}} \end{pmatrix}\begin{pmatrix} v_x \\ v_y \end{pmatrix}, \tag{44}$$

with the conductivity

$$\sigma_{xx} = \frac{\frac{ne^2\tau^{\parallel}}{m}}{1+(\frac{eB}{m}+\frac{1}{\tau^{\perp}})^2\tau^{\parallel 2}}, \quad \sigma_{xy} = -\frac{ne^2(eB+\frac{m}{\tau^{\perp}})\frac{\tau^{\parallel 2}}{m^2}}{1+(\frac{eB}{m}+\frac{1}{\tau^{\perp}})^2\tau^{\parallel 2}}, \tag{45}$$

which gives the same result as that in the Boltzmann theory Eq. 23 when considering only the skew scattering part. In Drude model, $m\mathbf{v}/\tau$ is a resistive force. The physical meaning of the anisotropic resistive force is that the direction of the force is no longer the same with that of the velocity. This anisotropic force in the Drude theory, on the other hand, is equivalent to the anisotropic scattering in the Boltzmann theory. The difference between Boltzmann theory and the Drude phenomenological theory is that the Drude theory cannot give a specific expression of the longitudinal and transverse relaxation time.

Converting the conductivity into resistivity, we get

$$\rho_{xx} = \frac{m}{e^2\tau^{\parallel}n}, \tag{46}$$

$$\rho_{xy} = -\left(\frac{B}{en} + \frac{m}{e^2\tau^{\perp}n}\right). \tag{47}$$

Based on our theory, from Eq. 21, we see that the magnetic field dependence of $\tau^{\parallel}$ contribute to the negative magnetoresistance, while $\frac{1}{\tau^{\perp}}$ contribute to the anomalous Hall effect.

V. CONCLUSION

In summary, we have formulated a classical theory for the magnetotransport in the 2D Lorentz model. This theory takes into account the effects of the magnetic field on the electron-impurity scattering using the recipe of the abstraction of the real scattering process in the classical Boltzmann framework. We find a correction to the Hall resistivity in the conventional Boltzmann-Drude theory and a negative magnetoresistivity as a parabolic function of magnetic field. The origin of these results has been analyzed. We have also discussed the relevance between our theory and recent simulation and experimental works.

We acknowledge useful discussions with Liuyang Sun, Liang Dong, Nikolai A. Sinitsyn, Qi Chen, Liang Du, Fengcheng Wu and Huaiming Guo. Q.N. is supported by DOE (DE-FG03-02ER45958, Division of Materials Science and Engineering) in the formulation of our theoy. J.F., C.X. and Y.G. are supported by NSF (EFMA-1641101) and Welch Foundation (F-1255).

Appendix A: Derivation of differential cross section

The relation between impact parameter b and the scattering angle θ in Eq. 1 is derived from the geometry of the scattering process shown in Fig. 9. The scattering angle θ is from $\mathbf{k}$ to $\mathbf{k}'$. Because the direction of $\mathbf{y}$-axis is $\frac{\pi}{2}$ larger than $\mathbf{k}$, and the direction of vector $\overrightarrow{EC'}$ is $\frac{\pi}{2}$ larger than $\mathbf{k}'$, the angle between vector $\overrightarrow{EC'}$ and the $\mathbf{y}$-axis is equal to the scattering angle θ. Equivalently, the angle between $\overrightarrow{AC}$ and $\overrightarrow{AC'}$ is equivalent to the scattering angle θ. Therefore, there is a relation

$$\frac{\theta}{2} = \pi - \angle OAC. \tag{A1}$$

Along with the cosine theorem for the $\angle OAC$: $a^2+R^2-2aR\cos\angle OAC = (b+R)^2$, there is

$$a^2 + R^2 + 2aR\cos\frac{\theta}{2} = (b+R)^2. \tag{A2}$$

Therefore, the expression of b in terms of θ is

$$b = -R + \sqrt{a^2+R^2+2aR\cos\frac{\theta}{2}}. \tag{A3}$$

For the inverse process $\mathbf{k}' \to \mathbf{k}$, the scattering angle is $2\pi-\theta$, which falls in the range of $[0, 2\pi]$. We only focus on the calculation within $[0, 2\pi]$, because the scattering has periodicity of 2π. Beyond $[0, 2\pi]$, the scattering process is the same in every 2π period. Substituting θ for $2\pi-\theta$ in Eq. A3, we get the differential cross section for $\mathbf{k}' \to \mathbf{k}$ process

$$b = -R + \sqrt{a^2+R^2-2aR\cos\frac{\theta}{2}}. \tag{A4}$$

As we see, the two process $\mathbf{k}' \to \mathbf{k}$ and $\mathbf{k} \to \mathbf{k}'$ have different differential cross section, which leads to skew scattering.

Appendix B: Derivation of coordinate jump

The coordinate jump can be derived by $\delta\mathbf{r} = \overrightarrow{OE} - \overrightarrow{OD}$, where D and E are the starting point and ending point (Fig. 9). $\overrightarrow{OE} = \overrightarrow{OC'} + \overrightarrow{C'E}$. $\overrightarrow{OC'} = -(R+$

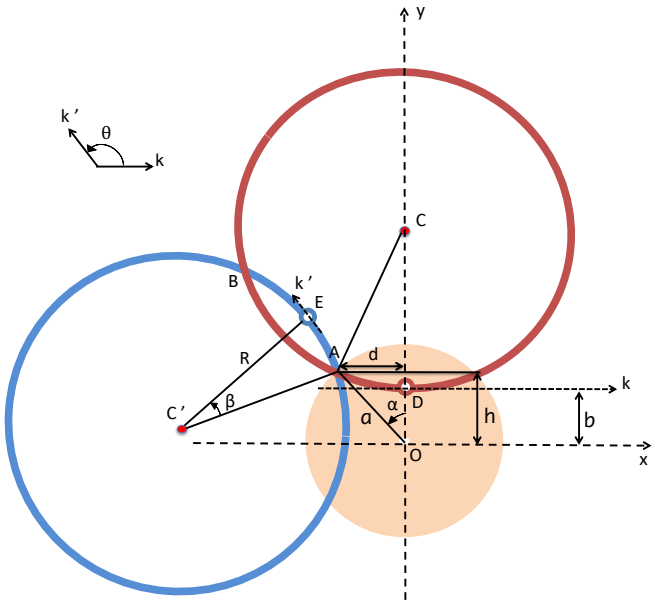

FIG. 9. The geometry of the scattering process in the presence of magnetic field. Point O is the center of impurity. Point C and C' are the center of the circle of the initial asymptote, and the circle of the final asymptote, respectively. Point A is the impact point on the scatterer boundary. Point D is the closest approach to the scatterer on the initial asymptote. Point E on the final asymptote is simultaneous with point D.

$b)\sin(2\alpha)\hat{\mathbf{x}} + (R+b)\cos(2\alpha)\hat{\mathbf{y}}$. $\overrightarrow{C'E} = R\sin(\theta)\hat{\mathbf{x}} - R\cos(\theta)\hat{\mathbf{y}}$. So $\overrightarrow{OE} = [-(R+b)\sin(2\alpha) + R\sin(\theta)]\,\hat{\mathbf{x}} + [(R+b)\cos(2\alpha) - R\cos(\theta)]\,\hat{\mathbf{y}}$.

Also, because $\overrightarrow{OD} = b\hat{\mathbf{y}}$, there are

$$\delta\mathbf{x} = [-(R+b)\sin(2\alpha) + R\sin(\theta)]\,\hat{\mathbf{x}}, \tag{B1}$$

$$\delta\mathbf{y} = [(R+b)\cos(2\alpha) - R\cos(\theta) - b]\,\hat{\mathbf{y}}. \tag{B2}$$

To replace b and α in terms of R, a, θ, we get

$$\delta\mathbf{x} = R\left[\sin\theta - \frac{\sin\theta + 2\frac{a}{R}\sin\left(\frac{\theta}{2}\right)}{\sqrt{1+\frac{2a}{R}\cos(\frac{\theta}{2})+\frac{a^2}{R^2}}}\right]\hat{\mathbf{x}}, \tag{B3}$$

$$\delta\mathbf{y} = 2R\sin^2\left(\frac{\theta}{2}\right)\left[1 - \frac{1}{\sqrt{1+\frac{2a}{R}\cos(\frac{\theta}{2})+\frac{a^2}{R^2}}}\right]\hat{\mathbf{y}}. \tag{B4}$$

Appendix C: Rigorous treatment of Boltzmann equation

In general, the Boltzmann equation can be written as

$$(-e)\left(\mathbf{E}+\mathbf{v}\times\mathbf{B}\right)\cdot\frac{\partial f_{\mathbf{k}}}{\hbar\partial\mathbf{k}} = -\int_0^{2\pi} d\theta\left[W_{\mathbf{k}\mathbf{k}'}f\left(\epsilon,\mathbf{k}\right)\left(1-f\left(\epsilon,\mathbf{k}'\right)\right) - W_{\mathbf{k}'\mathbf{k}}f\left(\epsilon,\mathbf{k}'\right)\left(1-f\left(\epsilon,\mathbf{k}\right)\right)\right], \tag{C1}$$

where $W_{\mathbf{k}\mathbf{k}'}$ is the probability of scattering from k to k'.

In a more rigorous treatment shown by Kohn and Luttinger in Eq. (21) of Ref. [28], it makes a correspondence between the classical distribution function and the quantum mechanical density matrix. In this treatment, the right hand side of Boltzmann equation becomes

$$(-e)\left(\mathbf{E}+\mathbf{v}\times\mathbf{B}\right)\cdot\frac{\partial f_{\mathbf{k}}}{\hbar\partial\mathbf{k}} = -\int_0^{2\pi} d\theta\left[W_{\mathbf{k}\mathbf{k}'}f\left(\epsilon,\mathbf{k}\right) - W_{\mathbf{k}'\mathbf{k}}f\left(\epsilon,\mathbf{k}'\right)\right]. \tag{C2}$$

This rigorous treatment in Boltzmann equation has been applied by previous literatures ([29], [30], etc.).

Appendix D: The contribution of differential cross section to relaxation time

Generally, we will prove that $\tau^{\parallel}$ is contributed purely by Ω^S, and $\tau^{\perp}$ is contributed purely by Ω^A. We first express the differential cross section as a function of scattering angle $f(\theta)$. Then, $\Omega^A = \frac{1}{2}(f(\theta) - f(2\pi-\theta))$, $\Omega^S = \frac{1}{2}(f(\theta) + f(2\pi-\theta))$. We prove that the term $\Omega^A(1+\cos(\theta))$ in Eq. 21 and $\Omega^S\sin(\theta)$ in Eq. 22 vanishes after integral by

$$\begin{aligned}
&\int_0^{2\pi} d\theta\Omega^A(1+\cos(\theta)) \\
&= \frac{1}{2}\int_0^{2\pi} d\theta(f(\theta)-f(2\pi-\theta))(1+\cos(\theta)) \\
&= \frac{1}{2}\int_0^{2\pi} d\theta f(\theta)(1+\cos(\theta)) \\
&\quad -\frac{1}{2}\int_{2\pi}^{0} d(2\pi-\theta)f(\theta)\sin(1+\cos(2\pi-\theta)) \\
&= 0,
\end{aligned} \tag{D1}$$

and

$$\begin{aligned}
&\int_0^{2\pi} d\theta \Omega^S \sin(\theta) \\
&= \frac{1}{2}\int_0^{2\pi} d\theta (f(\theta) + f(2\pi-\theta)) \sin(\theta) \\
&= \frac{1}{2}\int_0^{2\pi} d\theta f(\theta) \sin(\theta) \\
&\quad + \frac{1}{2}\int_{2\pi}^{0} d(2\pi-\theta) f(\theta) \sin(2\pi-\theta) \\
&= 0.
\end{aligned} \tag{D2}$$

Therefore, we have demonstrated that the symmetric and antisymmetric part of the probability of scattering contribute to the conventional transport relaxation time $\tau^{\parallel}$ and the transverse relaxation time $\tau^{\perp}$, respectively.

Appendix E: Application to soft potential under magnetic field

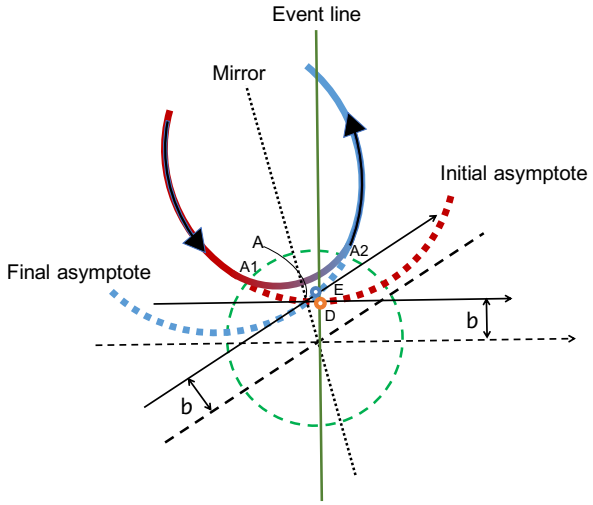

FIG. 10. The plot of soft potential scattering. The green dashed circle is the range, within which the potential influences on. The real trajectory, incoming with red solid curve and outgoing with blue solid curve, intersects the green dashed circle at two points $A1$ and $A2$. The red dashed curve and blue dashed curve are the initial asymptote and final asymptote, respectively. A is the crossing point between the red and blue dashed curve. The incoming trajectory and the outgoing trajectory are symmetric about the mirror line, which passes through point A and the scatterer center. The red dot D is the starting point on the event line, and the blue dot E is the ending point that is at the same time with the event line.

We here demonstrate how to apply our abstraction method to the soft potential scattering in magnetic field. We assume a central soft potential with a well-defined center of scattering. The soft potential goes to zero at infinity. As a result, we can draw a circle (green dashed circle) around the potential center that is large enough so that the interaction between electron and potential outside the circle is negligible (See Fig. 10). The real trajectory intersects the green dashed circle at two points $A1$ and $A2$. Before reaching $A1$ and after reaching $A2$, the real trajectory coincides with the initial and final asymptote, respectively. We then extend the initial and final asymptote after $A1$ and before $A2$ to their intersecting point A. The time from A to $A1$ and A to $A2$ are the same, due to the mirror symmetry. The mirror symmetry is proven by the following. The angular momentum outside the green circle $\mathbf{L}$ satisfies

$$\begin{aligned}
\frac{d\mathbf{L}}{dt} &= \mathbf{r} \times m\dot{\mathbf{v}} \\
&= \mathbf{r} \times (-e\dot{\mathbf{r}} \times \mathbf{B}) \\
&= -e(\mathbf{r}\cdot\dot{\mathbf{r}})\mathbf{B} \qquad \text{(E1)} \\
&= -\frac{d}{dt}(\frac{1}{2}er^2\mathbf{B}).
\end{aligned}$$

(E2)

Therefore, the quantity $\mathbf{r}\times m\mathbf{v} + \frac{1}{2}er^2\mathbf{B} = constant$. The $\frac{1}{2}er^2\mathbf{B}$ is constant on the green circle, because $|r_1| = |r_2| = R$. Therefore, the angular momentum $\mathbf{r}\times m\mathbf{v}$ is constant at A_1 and A_2. Due to energy conservation, $|\mathbf{v_1}| = |\mathbf{v_2}|$. Therefore, the velocity at A_1 and A_2 are symmetric (if reversing the velocity at A_2 by π) about the mirror line which passes through the intersection of the elongated velocity of A_1 and A_2. The intersection of the initial and final asymptote A falls on the mirror line as well.

We can define the starting point and ending point in a similar fashion. The starting point, marked as D (red dot) in Fig. 10, is the closest approach to the center of scatterer on the initial asymptote. The event line, connecting the starting point and the center of the scatterer, marks the occurring of scattering event. The blue dot on the final asymptote is the ending point E, which satisfies that the time from A to D and A to E are the same. By definition, both D and E are on the asymptote, not on real trajectory. Therefore, the ending point E is not influenced by the scattering potential. The purpose of our method is to provide a way to appropriately parametrize the scattering process.

In summary, the electron motion in a soft potential and magnetic field can be abstracted as follows. The electron moves along the initial asymptote to the starting point, gets scattered to the ending point and finally moves away from the scatterer along the final asymptote. The initial asymptote, final asymptote and the event line have the same definition with those defined in the manuscript with the hard disk potential.

As discussed in Section III B, the finite impurity range (green dashed circle) is the key to differentiate the magnetoresistance from Drude theory at low magnetic fields. For both hard disk potential and soft potential, the larger the impurity range, the more significant influence it has on the resistivity.

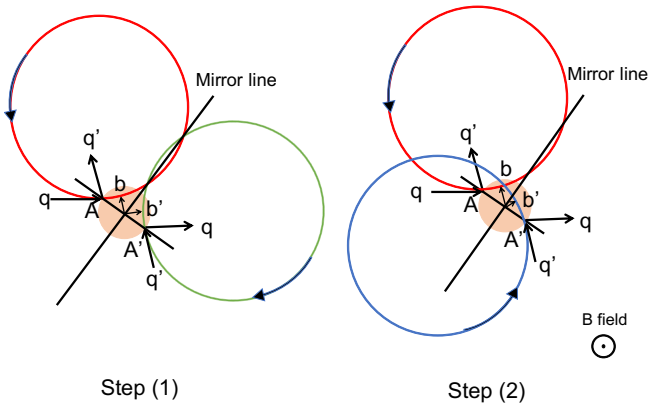

FIG. 11. The sketch of scattering process from $\mathbf{q} \to \mathbf{q}'$ and $\mathbf{q}' \to \mathbf{q}$ process: (1) with symmetric scattering angle θ and symmetric impact parameter $b = b'$ due to reversed magnetic field; (2) with symmetric scattering angle θ but different impact parameter $b \neq b'$ due to correct magnetic field direction. The left side of mirror line plots the $\mathbf{q} \to \mathbf{q}'$ process, and the right side of mirror line plots the $\mathbf{q}' \to \mathbf{q}$ process. A and A' are the impact point at each side. b and b' are the impact parameter at each side. In step (1) with reversed magnetic field direction, the $\mathbf{q} \to \mathbf{q}'$ and $\mathbf{q}' \to \mathbf{q}$ process are symmetric with respect to the mirror line. Step (2) plots $\mathbf{q}' \to \mathbf{q}$ process with correct magnetic field direction. The impact parameter b' is no longer the same with b.

Appendix F:

Alternative understanding of anisotropic scattering

We can use the impact point on the boundary of scatterer to understand how differential cross section is different between $\mathbf{q} \to \mathbf{q}'$ and $\mathbf{q}' \to \mathbf{q}$ process, using the following two steps as shown in Fig. 11 (where $\mathbf{q}$ and $\mathbf{q}'$ are the momentum on the scatterer boundary). (1): We first draw the incoming trajectory for $\mathbf{q} \to \mathbf{q}'$ process. We then draw a line crossing the center of scatterer and parallel to the tangent line at the impact point A as mirror line. We then draw the mirror image of the $\mathbf{q} \to \mathbf{q}'$ process at right side of the mirror line (Fig. 11, step (1)). The impact point goes to A' which is the mirror image of A. Now the impact parameter is the same for the two processes, i.e. $b = b'$, which gives no skew scattering. (2): The magnetic field direction determines that the rotation of electron should be counterclockwise. However, upon doing step (1), the rotation is clockwise in $\mathbf{q}' \to \mathbf{q}$ process, which is incorrect. The correct way for $\mathbf{q}' \to \mathbf{q}$ is to draw the counterclockwise trajectory tangential to the incident and scattered momentum at A' (we only show the incident trajectory in Fig. 11, step (2)). It is clear that the impact parameter b' is different from b, which generates asymmetry between $\mathbf{q} \to \mathbf{q}'$ and $\mathbf{q}' \to \mathbf{q}$ process. While the scattering angle stays the same, the differential cross section is different due to $\Omega = |db/d\theta|$. This analysis also shows the role of the magnetic field in the skew scattering. The $\mathbf{q}' \to \mathbf{q}$ process in step (1) reverses the direction of the magnetic field. In order to correct this, the electron trajectory has to be subject to another mirror/time reversal operation as in step (2). The resulting correct $\mathbf{q}' \to \mathbf{q}$ process is thus no longer symmetric with the original $\mathbf{q} \to \mathbf{q}'$ process.

[1] L. D. Landau, and E. M. Lifshitz, Physics Kinetics (Butterworth-Heinemann, 2012).
[2] A. A. Abrikosov, Phys. Rev. B **58**, 2788 (1998).
[3] L. Boltzmann, Annalen der Physik **241**, 430–432 (1878).
[4] A. V. Bobylev, F. A. Maaø, A. Hansen, and E. H. Hauge, Phys. Rev. Lett. **75**, 197 (1995).
[5] A. V. Bobylev, F. A. Maaø, A. Hansen, and E. H. Hauge, J. Stat. Phys. **87**, Nos. 5/6. (1997).
[6] A. Dmitriev, M. Dyakonov, and R. Jullien, Phys. Rev. Lett. **89**, 266804 (2002).
[7] V. V. Cheianov, A. P. Dmitriev, and V. Yu. Kachorovskii, Phys. Rev. B **68**, 201304(R) (2003); **70**, 245307 (2004).
[8] A. P. Dmitriev, and V. Yu. Kachorovskii, Phys. Rev. B **77**, 193308 (2008).
[9] H. I. Cho, G. M. Gusev, Z. D. Kvon, V. T. Renard, J. H. Lee, and J. C. Portal, Phys. Rev. B **71**, 245323 (2005).
[10] J. Smit, Physica A: Statistical Mechanics and its Applications **24**, 39-51 (1958).
[11] L. Berger, Phys. Rev. B **2**, 4559–4566 (1970).
[12] W. Götze, E. Leutheusser, and S. Yip, Phys. Rev. A **25**, 533–539 (1982).
[13] R. Kubo, J. Phys. Soc. Jpn. **12**, 570-586 (1957).
[14] R. P. Cowburn, A. O. Adeyeye, and J. A. C. Bland, Appl. Phys. Lett. **70**, 2309 (1997).
[15] A. D. Mirlin, D. G. Polyakov, F. Evers, and P. Wölfle, Phys. Rev. Lett. **87**, 126805 (2001).
[16] D. Weiss, Transport in Antidot Superlattices (Kluwer Academic Publishers 1995).
[17] V. Renard, Z. D. Kvon, G. M. Gusev, and J. C. Portal. Phys. Rev. B 70, 033303 (2004).
[18] M. Flser, B. A. Piot, C. L. Campbell, D. K. Maude, M. Henini, R. Airey, Z. R. Wasilewski, S. Florens and T. Champel, New J. Phys 15, 083027 (2013).
[19] M. M. Fogler, A. Yu. Dobin, V. I. Perel, and B. I. Shklovskii. Phys. Rev. B 56, 6823 (1997).
[20] D. G. Polyakov, F. Evers, A. D. Mirlin, and P. Wlfle. Phys. Rev. B 64, 205306 (2001).
[21] M. Tornow, D. Weiss, K. v. Klitzing, K. Eberl, David J. Bergman, and Yakov M. Strelniker, Phys. Rev. Lett. **77**, 147 (1996).
[22] B. L. Altshuler, D. Khmel'nitzkii, A. I. Larkin, and P. A. Lee, Phys. Rev. B **22**, 5142 (1980).
[23] N. A. Sinitsyn, Q. Niu, J. Sinova and K. Nomura, Phys. Rev. B **72**, 045346 (2005).

[24] N. A. Sinitsyn, Q. Niu, and A. H. MacDonald, Phys. Rev. B **73**, 075318 (2006).
[25] Y. Gao, S. A. Yang, and Q. Niu, Phys. Rev. Lett. **112**, 166601 (2014).
[26] A. P. Dmitriev, M. Dyakonov, and R. Jullien, Phys. Rev. B **64**, 233321 (2001).
[27] N. M. Sotomayor, G. M. Gusev, J. R. Leite, A. A. Bykov, A. K. Kalagin, V. M. Kudryashev, and A. I. Toropov, Phys. Rev. B **70**, 235326 (2004).
[28] W. Kohn and J. M. Luttinger, Phys. Rev. **108**, 590 (1957).
[29] H. Chen, Y. Gao, D. Xiao, A. H. MacDonald, and Q. Niu, arXiv: 1511.02557v1 (2015).
[30] G. Sundaram and Q. Niu, Phys. Rev. B **59**, 14915 (1999).